International Journal of Mechanical, Industrial and Aerospace Sciences
ISSN: 2517-9950
Vol:5, No:8, 2011

Thermal Post-buckling of Shape Memory Alloy Composite Plates under Non-uniform Temperature Distribution

Z.A. Rasid, R. Zahari, A. Ayob, D.L. Majid, and A.S.M. Rafie

***Abstract*—**Aerospace vehicles are subjected to non-uniform thermal loading that may cause thermal buckling. A study was conducted on the thermal post-buckling of shape memory alloy composite plates subjected to the non-uniform tent-like temperature field. The shape memory alloy wires were embedded within the laminated composite plates to add recovery stress to the plates. The non-linear finite element model that considered the recovery stress of the shape memory alloy and temperature dependent properties of the shape memory alloy and composite matrix along with its source codes were developed. It was found that the post-buckling paths of the shape memory alloy composite plates subjected to various tent-like temperature fields were stable within the studied temperature range. The addition of shape memory alloy wires to the composite plates was found to significantly improve the post-buckling behavior of laminated composite plates under non-uniform temperature distribution.

***Keywords*—**Post-buckling, shape memory alloy, temperature dependent property, tent-like temperature distribution

I. Introduction

THE existence of thermal loading that is contributed by non-uniform aerodynamic and solar radiation heating has increased the significance of thermal buckling problem of composite members of aerospace structures. Studies on the thermal buckling of composite plates that covered great understanding on the subject were conducted by researchers in [1] and [2]. A work on the thermal buckling due to the non-uniform temperature field was studied by Chen et al [3] and later Chen and Chen [4] further the work on the thermal post-buckling of laminated composite plates. The results showed that the thermal post-buckling subjected to the tent-like temperature distribution was influenced by lamination angle, plate aspect ratio, modulus ratio, and the number of layers. In recent years, smart materials such as piezoelectric and shape memory alloy (SMA) have been used to improve the buckling behavior of composite structures. Nezamabadi and Khorramabadi in [5], [6] used a pair of piezoelectric layers to improve buckling behavior of Engesser-Timoshenko and functionally graded beams. The method of improvements of composite structural behaviors by embedding SMA wires within those structures can be classified as active property tuning (APT) and active strain energy tuning (ASET) [7]. Kumar and Singh [8] applied a layerwise theory of composite plates to study the effect of varying several composite parameters such as the side-thickness ratio, fiber orientation and boundary condition on the thermal buckling of the uniformly heated SMA composite plates. It was found that the critical temperatures were enhanced by the addition of the SMA. The studies on the effect of SMA on the thermal post-buckling behavior of laminated composites subjected to uniform temperature distribution were conducted by Tawfik et al [9] and Park et al [10]. The effects of SMA parameters such as the initial strain and the volume fraction of the embedded SMA were studied. It was proven that SMA wires can significantly improve the post-buckling behavior of laminated composites.

Z. A. Rasid is with the Mechanical Engineering Department, University Technology of Malaysia, Kuala Lumpur, 84100 MALAYSIA (phone: 603-2615-4000; fax: 603-2615-4315; e-mail: zainudin@ic.utm.my).

R. Zahari, is with the Aerospace Engineering Department, University Putra of Malaysia, Serdang, 43400 MALAYSIA (e-mail: rizal@eng.upm.edu.my).

A. Ayob is with the Mechanical Engineering Faculty, University Technology of Malaysia, Skudai, 81300 Malaysia (e-mail: amran@fkm.utm.my).

II. Simulation

The finite element formulation developed here used the strength of material approach where stress term due to the recovery stress of the SMA was added to the constitutive relationship [11].

A. Strains

Using the Mindlin's first order shear deformation theory [12] while including the von Karman's strain terms in the equation, the incremental strain vector can be expressed as

$$\{\Delta\varepsilon\} = \begin{Bmatrix}\Delta\varepsilon_x\\ \Delta\varepsilon_x\\ \Delta\gamma_{xy}\end{Bmatrix} = \frac{1}{2}\begin{Bmatrix}\left(\frac{\partial \Delta w}{\partial x}\right)^2\\ \left(\frac{\partial \Delta w}{\partial y}\right)^2\\ 2\left(\frac{\partial \Delta w}{\partial x}\right)\left(\frac{\partial \Delta w}{\partial y}\right)\end{Bmatrix} + \begin{Bmatrix}\frac{\partial \Delta u}{\partial x}\\ \frac{\partial \Delta v}{\partial y}\\ \frac{\partial \Delta u}{\partial y}+\frac{\partial \Delta v}{\partial x}\end{Bmatrix} + \begin{Bmatrix}\left(\frac{\partial \Delta w}{\partial x}\right)\left(\frac{\partial w_0}{\partial x}\right)\\ \left(\frac{\partial \Delta w}{\partial y}\right)\left(\frac{\partial w_0}{\partial y}\right)\\ \left(\frac{\partial \Delta w}{\partial x}\right)\left(\frac{\partial w_0}{\partial y}\right)+\left(\frac{\partial \Delta w}{\partial y}\right)\left(\frac{\partial w_0}{\partial x}\right)\end{Bmatrix} + z\begin{Bmatrix}\frac{\partial \Delta\theta_x}{\partial x}\\ \frac{\partial \Delta\theta_y}{\partial y}\\ \frac{\partial \Delta\theta_x}{\partial y}+\frac{\partial \Delta\theta_y}{\partial x}\end{Bmatrix} \quad (1)$$

or

$$\{\Delta\varepsilon\} = \{\Delta\varepsilon_p\} + z\{\Delta\kappa\}$$

$$= \{\Delta\varepsilon_m\} + \{\Delta\varepsilon_{nl}\} + \{\Delta\varepsilon_o\} + z\{\Delta\kappa\} \quad (2)$$

where $\{\Delta\varepsilon_m\}$, $\{\Delta\varepsilon_{nl}\}$, $\{\Delta\varepsilon_o\}$, and $\{\Delta\kappa\}$ are the incremental in-plane linear strain vector, incremental in-plane nonlinear strain vector, incremental in-plane vector due to initial deflection, and the incremental curvature strain vector, respectively. Furthermore Δu,Δv, and Δw are the incremental displacements in the *x*, *y*, and *z* directions respectively. w_0,$\Delta\theta_x$, and $\Delta\theta_y$ are the total initial deflection, incremental rotation in the *x*-*z* plane, and the incremental rotation in the *y*-*z* plane respectively.

B. Constitutive Relationship

The constitutive relationship in terms of stress resultants are

$$\begin{Bmatrix} N \\ M \end{Bmatrix} = \begin{bmatrix} A & B \\ B & D \end{bmatrix}\left(\begin{Bmatrix} \Delta\varepsilon_l \\ \Delta\kappa \end{Bmatrix} + \begin{Bmatrix} \Delta\varepsilon_{nl} \\ 0 \end{Bmatrix} + \begin{Bmatrix} \Delta\varepsilon_0 \\ 0 \end{Bmatrix}\right) - \begin{Bmatrix} N^{\Delta T} \\ M^{\Delta T} \end{Bmatrix} + \begin{Bmatrix} N_0 \\ M_0 \end{Bmatrix} \qquad T < A_s \quad (3a)$$

$$= \begin{bmatrix} A & B \\ B & D \end{bmatrix}\left(\begin{Bmatrix} \Delta\varepsilon_l \\ \Delta\kappa \end{Bmatrix} + \begin{Bmatrix} \Delta\varepsilon_{nl} \\ 0 \end{Bmatrix} + \begin{Bmatrix} \Delta\varepsilon_0 \\ 0 \end{Bmatrix}\right) - \begin{Bmatrix} N^{\Delta T} \\ M^{\Delta T} \end{Bmatrix} + \begin{Bmatrix} N^{\Delta r} \\ M^{\Delta r} \end{Bmatrix} + \begin{Bmatrix} N_0 \\ M_0 \end{Bmatrix} \qquad T \geq A_s \quad (3b)$$

where

$$([A],[B],[D]) = \sum_{k=1}^{n}\int [\bar{Q}]_k(1, z, z^2)\, dz \quad (4)$$

For $T < A_s$,

$$\left(\{N^{\Delta T}\},\{M^{\Delta T}\}\right) = \sum_{k=1}^{n}\int \Delta T[\bar{Q}]_k\{\alpha\}(1, z)\, dz \quad (5a)$$

whereas for $T \geq A_s$,

$$\left(\{N^{\Delta T}\},\{M^{\Delta T}\}\right) = \sum_{k=1}^{n}\int V_m\Delta T[\bar{Q}]_m\{\alpha\}(1, z)\, dz \quad (5b)$$

$$\left(\{N^{\Delta r}\},\{M^{\Delta r}\}\right) = \sum_{k=1}^{n}\int V_a\{\sigma^r\}(1, z)\, dz \quad (6)$$

$\{N\}$ and $\{M\}$ are the force and moment resultant vectors respectively while $[A]$, $[B]$, and $[D]$ are the laminate stiffness matrices. $\{N^{\Delta T}\}$ and $\{M^{\Delta T}\}$ are the incremental resultant force and moment vectors due to the change in temperature respectively. $\{N^{\Delta r}\}$ and $\{M^{\Delta r}\}$ are the resultant force and moment vectors due to the recovery stress, respectively. $\{N_0\}$ and $\{M_0\}$ are the initial force and moment vectors respectively. n is the number of layer of the composite plate. The transverse force resultant vector is

$$\{S\} = \begin{Bmatrix} S_{xz} \\ S_{yz} \end{Bmatrix} = \begin{bmatrix} V_{44} & V_{45} \\ V_{45} & V_{55} \end{bmatrix}\{\Delta\gamma\} + \begin{Bmatrix} S_{xz0} \\ S_{yz0} \end{Bmatrix} = [V]\{\Delta\gamma\} + \{S_0\} \quad (7)$$

where

$$(V_{44}, V_{45}, V_{55}) = \sum_{k=1}^{n}\int (\bar{Q}_{44}, \bar{Q}_{45}, \bar{Q}_{55})\, dz \quad (8)$$

C. Finite Element Implementation

Serendipity elements each with eight nodes were used in this study. The finite element method governing equation for the thermal post-buckling of SMA composite plates is

$$\left([K_L] + [K_s] - [K_{\Delta T}] + [K_{\Delta r}] + [K_0] + [K_{w0}] + \frac{1}{2}[N1] + \frac{1}{2}[N1_{w0}] + \frac{1}{3}[N2]\right)\{\Delta q\} = \{P_{\Delta T}\} - \{P_{\Delta r}\} - \{P_0\} - \{P_{w0\Delta T}\} - \{P_{w0\Delta r}\} - \{P_{0w0}\} \quad (9)$$

where $\{\Delta q\}$ is the incremental nodal displacement vector. $[K_L]$ and $[K_s]$ are the linear membrane and shear stiffness matrices, respectively. $[K_{\Delta T}]$ and $[K_{\Delta r}]$ are the incremental temperature and recovery stress matrices respectively. $[K_0]$ and $[K_{w0}]$ are the initial stiffness and the initial stiffness due to initial deflection matrices, respectively. $[N1]$, $[N1_{w0}]$, and $[N2]$ are the first order non-linear stiffness, first order non-linear stiffness due to initial deflection and the second order stiffness matrices respectively. $\{P_{\Delta T}\}$ and $\{P_{\Delta r}\}$ are the incremental temperature and recovery force vectors respectively. $\{P_{w0\Delta T}\}$, $\{P_{w0\Delta r}\}$ and $\{P_{0w0}\}$ are the vectors of forces due to the coupling of initial deflection and temperature increment, initial deflection and recovery stress increment and initial deflection and initial load respectively. Equation (9) was solved using the Newton-Raphson's method.

D. The Tent-like Temperature Field

With reference to Fig. 1, the tent-like temperature field was

$$T(x, y, z) = \begin{cases} T_0 + 2T_1\left(\frac{y}{b}\right), & 0 \leq y \leq \frac{b}{2} \\ T_0 + 2T_1\left(1 - \frac{y}{b}\right), & \frac{b}{2} \leq y \leq b \end{cases} \quad (10)$$

T_0 is the part of uniform temperature rise whereas T_1 is the temperature gradient.

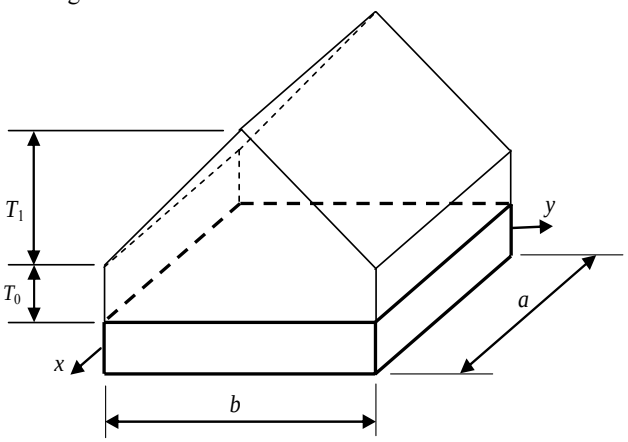

Fig. 1 The non-uniform tent-like temperature distribution

E. Dimensions and Properties

In this study, the anti-symmetric angle-ply composite plates with the configuration of $[45/-45]_6$ were analyzed. Nitinol wires with volume fraction of 5% were embedded in the graphite direction within a pair of outside layers of the SMA composite plates. As such, we have a pair of nitinol-graphite epoxy (N-GE) layers and others graphite-epoxy (GE) layers. Fig. 2 shows the diagram of such a plate.

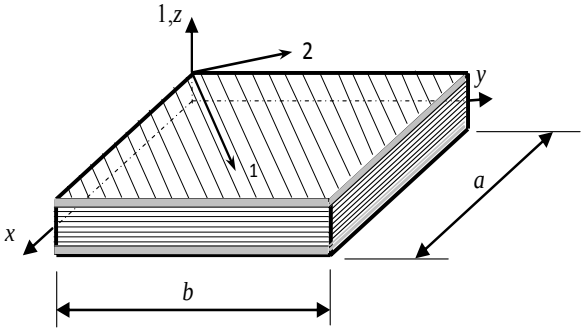

Fig. 2 The shape memory alloy composite plate (: GE layer, : N-GE)

The dimension of the plate was 100 mm x 100 mm with the length to thickness ratio, $\frac{a}{t} = 200$. The properties for the graphite-epoxy and SMA are given in Table 1. Notice that the properties for epoxy are temperature dependent where dT is the change of temperature.

TABLE I
PROPERTIES OF MATRIX GE AND NITINOL SMA

Property	Matrix GE	Nitinol SMA
Young's Modulus (GPa)	E_1=40(1-3.53(10^{-4}) dT) E_2=1-4.27(10^{-4}) dT	From Fig. 3 [13]
Shear Modulus (GPa)	G_{12} = 0.6(1-6.06(10^{-4}) dT) G_{13} =0.5(1-6.06)(10^{-4}) dT) G_{23} = G_{13}	G = 24.86 $T < A_s$ = 25.77 $T > A_s$
Poisson's Ratio	ν_{12} = 0.22	ν = 0.33
Thermal coefficient (1/^{0}C)	α_1= -0.07(10^{-6})(1-1.25(10-3) dT) α_2= 30.1(10^{-6})(1+0.41(10-3) dT)	α= 10.26(10^{-6})
Recovery Stress, σ_{rec} (MPa)	-	From Fig, 4 [13]
Austenite start temperature, A_s (^{0}C)	-	37.78

In this study, the simply supported (SS), the immovable edges (HH) and the clamped on all sides (CC) boundary conditions such as given below, with reference to Fig. 2 were used.

SS - at x=0, a: u=w=θ_y=0, at y=0, b: v=w=θ_x=0

HH - at x=0, a: u=v=w=θ_y=0, at y=0, b: u=v=w=θ_x=0

CC - at x=0, a and y=0, b: u=v=w=θ_x=θ_y=0

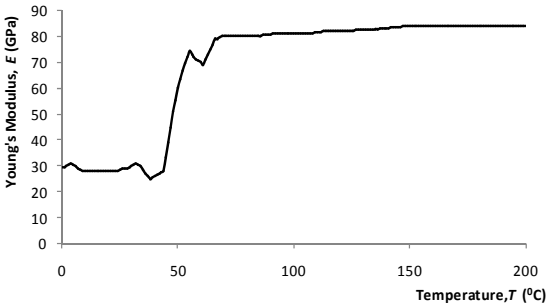

Fig. 3 The Young's modulus of the SMA over temperatures [13]

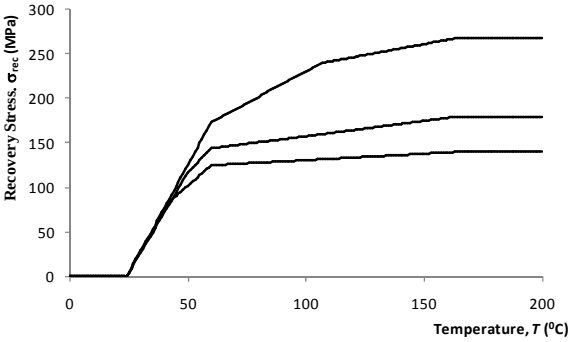

Fig. 4 The recovery stress of the SMA over temperatures for different initial strain, ε_0 [13]

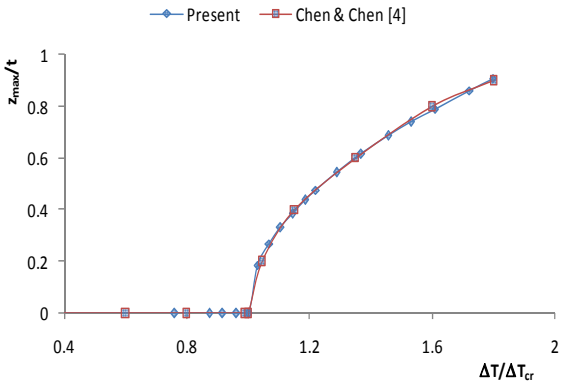

Fig. 5 The post-buckling path of the composite plate subjected to the tent-like temperature distribution

III. RESULTS AND DISCUSSION

A. Validations

A post-buckling analysis of a composite plate was conducted and the result was validated with the work of Chen and Chen [4]. The configuration of the plate was $[-30/30]_6$ whereas the SS boundary condition was used. The following properties and dimensions were applied:

$E_1/E_2 = 40$, $\nu_{12} = 0.25$, $G_{12}/E_2 = 0.5$, $\alpha_1 = \alpha_2 = 1.0(10^{-6})$
Geometry: $a = b = 0.1$ m, $a/t = 100$, $T_0 = 0.0\ ^0$C

Fig. 5 shows that the plot of the ratio of the maximum transverse displacement over thickness of the plate (z_{max}/t) against the ratio of the change of temperature over the critical temperature change ($\Delta T/\Delta T_{cr}$) of the composite plate subjected to the tent-like temperature distribution in the present analysis agreed excellently to the result of Chen and Chen [4].

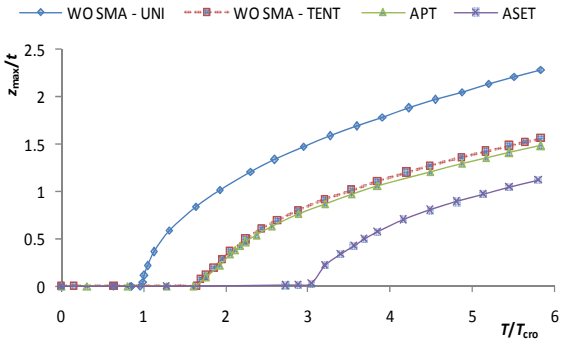

(a)

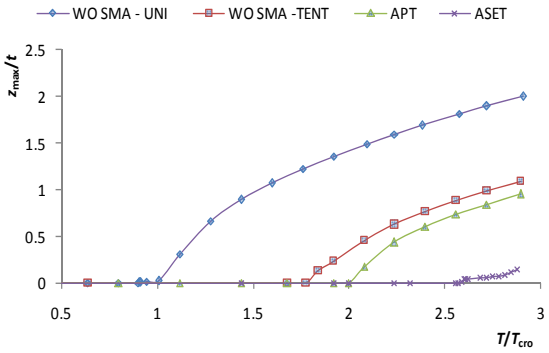

(b)

Fig. 6 Post-buckling paths of anti-symmetric composite plates subjected to tent-like temperature distribution (To = 0) for boundary conditions of (a) HH (b) CC

B. The Post-buckling Paths

Post-buckling analyses were firstly conducted on composite plates under uniform temperature distribution (WO SMA–UNI) and composite plates under the tent-like temperature distribution (WO SMA–TENT). Then applying the tent-like temperature distribution, the post-buckling analyses were conducted on SMA composite plates without the induced recovery stress (APT) and SMA compossite plates with the induced recovery stress (ASET). 2 types of the tent-like temperature fields in forms of $T_0 = 0$ and $T_1/T_0 = 1$ were considered whereas the boundary conditions considered were the HH and CC boundary conditions. The initial strain of $\varepsilon_0 = 1\%$ was applied. The plots of the ratio z_{max}/t against the ratio T/T_{cr0} are shown for the cases of $T_0 = 0$ (Fig. 6) and $T_1/T_0 = 1$ (Fig. 7) where T_{cr0} and z_{max} are the critical temperature for the case of WO SMA–UNI and the maximum transverse deflection of the plates respectively.

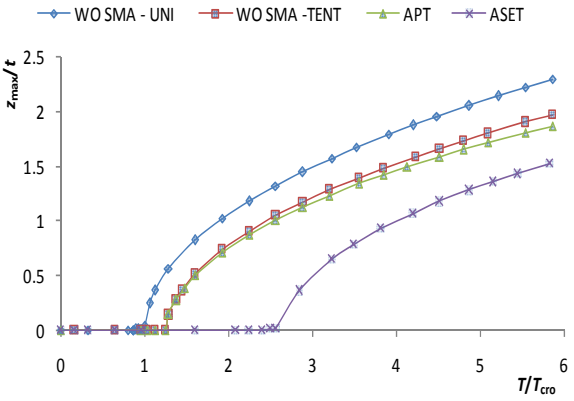

(a)

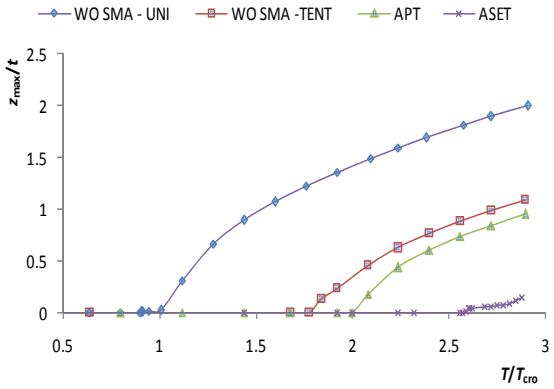

Fig. 7 Post-buckling paths of anti-symmetric composite plates subjected to the tent-like temperature distribution ($T_1/T_0 = 1$) for boundary conditions of (a) HH (b) CC.

From Fig. 6, stable post-buckling paths can be seen to occur in all cases of the analyses within the studied temperature range. Bifurcation occurs at $T/T_{cro} = 1$ for the case of WO SMA-UNI. Comparing the cases of WO SMA-UNI and WO SMA-N UNI, the non-uniform temperature distribution with $T_0 = 0$ has shifted the post-buckling path of the plate to the right. The effect of SMA can be seen to be significant in the ASET cases of both HH and CC boundary conditions while the effect of SMA in the case of APT is quite significant in the case CC boundary condition as compared to the case of HH boundary condition. In general, the HH boundary condition gave the higher effect of SMA where the bifurcation occurred at $T/T_{cro} = 3$ as in Fig. 6(a) as compared to its CC counter-part where $T/T_{cro} = 2.5$ such as shown in Fig. 6(b).

With reference to Fig. 7 that corresponds to the case of the tent-like temperature distribution with $T_1/T_0 = 1$, stable post-buckling paths can be seen to occur in all cases. Here the non-

uniform temperature distribution has cause less shifting of the post-buckling path of the plate as compared to the previous case of T_0 = 0. The effect of SMA can be seen to remain significant in the cases of ASET for both HH and CC boundary conditions. Fig. 7(a) shows the HH boundary condition still gave the higher effect of SMA where the bifurcation occurred at T/T_{cro} = 2.5 while the CC boundary condition caused bifurcation to occur at T/T_{cro} = 2.2 such as shown in Fig. 7(b).

C. The Effect of the Non-uniform Temperature Distribution

The post-buckling analyses of SMA composite plates were conducted for three values of T_1/T_0 to see the effect of the non-uniform temperature distribution on the post-buckling paths of composite plates. The plots of the ratio z_{max}/t against temperature, T are given in Fig. 9(a) that correspond to the APT case and in Fig. 9(b) that corresponds to the ASET case. It can be seen in both cases of APT and ASET, the post-buckling paths improved (shifted to the right) with the increased of the temperature. While the CC boundary condition gave the better post-buckling paths compared to the HH boundary conditions, both boundary conditions provide the same pattern of post-buckling plots in terms of the effect of T_1/T_0 whereas the T_1/T_0 ratio is increased, the plots are shifted more to the right.

IV. Conclusion

Thermal post-buckling analyses were conducted on the anti-symmetric SMA composite plates under non-uniform tent-like temperature distribution. The non-linear finite element model and its source codes were developed for theses analyses. For each analysis, four cases of WO SMA–UNI, WO SMA-N UNI, APT, and ASET were considered. It was found that under the non-uniform temperature loadings, post-buckling paths of SMA composite plates were stable. The effect of SMA on the thermal post-buckling paths was much significant in the ASET method as compared to the APT method. Even though the CC boundary condition gave higher bifurcation points, the effect of SMA was greater in the case of HH boundary condition where for example in the case of T_0 = 0, bifurcation point occurred at T_1/T_{cr0} = 3 for the HH boundary condition as compared to T_1/T_{cr0} = 2.5 for the CC boundary condition. Furthermore it was shown that with the increase of the ratio of T_1/T_0, the post-buckling paths improved (shifted to the right) for cases of APT and ASET with HH and CC boundary conditions.

Acknowledgment

This work is supported by the Malaysia's Ministry of Higher Education, FRGS grants (Vote 78700). Z.A. Rasid thanks the Ministry and the University Technology of Malaysia for their great support.

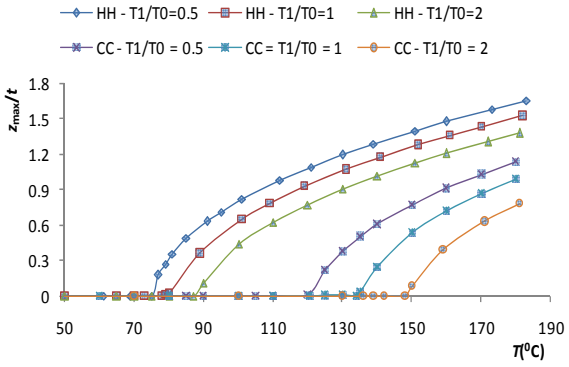

(a)

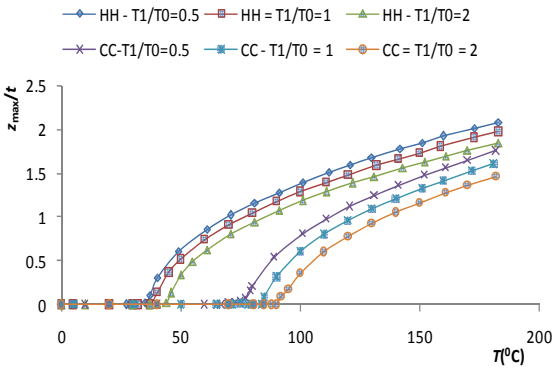

(b)

Fig. 8 The effect of temperature distribution on the post-buckling paths of SMA composite plates for the cases of (b) APT and (b) ASET

References

[1] J. S. Chang, "FEM analysis of buckling and thermal buckling of antisymmetric angle-ply laminates according to transverse shear and normal deformable high order displacement theory", *Computer and Structures*, vol. 37, pp. 925–946, 1990

[2] M. R. Prabhu and R. Dhanaraj, "Thermal buckling of laminated composite plates", *Computer and Structures*, vol. 53, pp. 1193–1204, 1994.

[3] W. J. Chen, P.D. Lin, and L. W. Chen, "Thermal buckling behavior of thick composite laminated plates under non-uniform temperature distribution", *Computer and Structures,* vol. 41, pp. 637– 645, 1991.

[4] L. W. Chen and L. Y. Chen, "Thermal Post-buckling analysis of laminated composite plates by the finite element method", *Composite and Structures*, vol. 12, pp. 257-270, 1989.

[5] A. R. Nezamabadi and M. K. Khorramabadi. "Mechanical Buckling of Engesser-Timoshenko Beams with a Pair of Piezoelectric Layers", *International Journal of Mechanical and Material*, vol. 1, pp. 106–109, 2010.

[6] M. K. Khorramabadi and A. R. Nezamabadi, "Stability of Functionally Graded Beams with Piezoelectric Layers Based on the First Order Shear Deformation Theory", *International Journal of Mechanical and Material*, vol. 1, pp. 131–134, 2010.

[7] C.A. Rogers, C. Liang and J. Jia, "Structural modification of simply supported laminated plates using embedded shape memory alloy fibres", *Computer and Structures,* vol. 38, pp. 569-580, 1991

[8] K. Kumar and B. N. Singh, "Thermal buckling analysis of SMA fiber-reinforced composite plates using layerwise model", *Journal of Aerospace Engineering*, vol. 22, pp. 342-353, 2009
[9] M. Tawfik, J.J. Ro and C. Mei, "Thermal post-buckling and aeroelastic behaviour of shape memory alloy reinforced plates", *Smart Material Structure*, vol. 11, pp. 297-307 2002.
[10] J. S. Park, J.H. Kim and S.H. Moon, "Thermal post-buckling and flutter characteristics of composite plates embedded with shape memory alloy fibers", *Composite Part B: Engineering*, vol. 36, pp. 627-636, 2005
[11] Z.A.Rasid, A. Ayob, R. Zahari, F. Mustapha, D.L. Majid and R. Varatharajoo, "Buckling and post-buckling improvements of laminated composite plates using finite element method", *Key Engineering Materials*, vol. 471-472, pp. 536-541, 2011.
[12] R. D. Mindlin, "Influence of rotary inertia and shear on flexural motions of isotropic elastic plates", *Journal of Applied Mechanics*, vol. 18, pp. 31-38, 1951
[13] W. B. Cross, A. H. Kariotis, and F. J. Stimler, Nitinol Characterization Study, NASA CR-1433, 1970.